AGU100 ADVANCING EARTH AND SPACE SCIENCE

Geophysical Research Letters

RESEARCH LETTER
10.1029/2019GL086387

How Tropical Convection Couples High Moist Static Energy Over Land and Ocean

Yi Zhang[1] and Stephan Fueglistaler[1,2]

[1]Program in Atmospheric and Oceanic Sciences, Princeton University, Princeton, NJ, USA, [2]Department of Geosciences, Princeton University, Princeton, NJ, USA

Key Points:
- The utility of quasi-equilibrium and weak temperature gradient theories (QE-WTG) can be demonstrated by a rainfall-weighting method
- Observed convection occurs at very similar subcloud moist static energy across all latitudes in the inner tropics as a result of QE-WTG
- The highest moist static energy values are tightly coupled over land and ocean, while the lower values are free to differ

Supporting Information:
- Supporting Information S1
- Supporting Information S2
- Figure S1
- Figure S2
- Figure S3
- Figure S4
- Figure S5

Correspondence to:
Y. Zhang,
yz8@princeton.edu

Citation:
Zhang, Y., & Fueglistaler, S. (2020). How tropical convection couples high moist static energy over land and ocean. *Geophysical Research Letters*, *47*, e2019GL086387. https://doi.org/10.1029/2019GL086387

Received 23 NOV 2019
Accepted 9 JAN 2020
Accepted article online 10 JAN 2020

Abstract We show that in the tropics, tropical atmospheric dynamics force the subcloud moist static energy (MSE) over land and ocean to be very similar in, and only in, regions of deep convection. Using observed rainfall as a proxy for convection and reanalysis data to calculate MSE, we show that subcloud MSE in the nonconvective regions may differ substantially between land and ocean but is uniform across latitudes in convective regions even on a daily timescale. This result holds also in CMIP5 model simulations of past cold and future warm climates. Furthermore, the distribution of rainfall amount in subcloud MSE is very similar over land and ocean with the peak at 343 J/g and a half width at half maximum of 3 J/g. Our results demonstrate that the horizontally uniform free tropospheric temperature forces the highest subcloud MSE values to be similar over land and ocean.

Plain Language Summary An extremely idealized picture of the tropical atmospheric dynamics is that deep convection sets a horizontally uniform free tropospheric temperature profile. Here, we show that despite the idealization, this simple picture is very useful in explaining the observations; convection occurs at very similar, spatially uniform subcloud MSE regardless of over land or ocean.

1. Introduction

The tropics show, even at equal latitudes and despite a relatively uniform annual mean insolation, a large variety of local climates ranging from regions with highest rainfall globally to deserts. Given the paramount importance of rainfall over land for ecosystems and humans, the processes governing its distribution and how it may change in the future are focus of intense efforts both in terms of improved process representations in numerical climate models and development of theories to interpret observations and model results (e.g., Byrne & O'Gorman, 2015; Lintner & Chiang, 2005; Pendergrass et al., 2017; Seneviratne et al., 2013). Understanding climate over land inevitably requires understanding its connection to the oceans. A fundamental difference between land and ocean is that over land, evapotranspiration is constrained by available moisture and, as a consequence, sensible heat flux plays a larger role over land than ocean. An important corollary of this surface energy budget consideration that is robustly observed in global climate model simulations is that the surface temperature response to radiative forcing is larger over land than ocean (Manabe et al., 1991).

The limited evaporation over land not only affects the partitioning between sensible and latent heat flux but also leads to different temperature lapse rates in the lower layers of the troposphere over land and ocean. Joshi et al. (2008) note that in model calculations there exists a level sufficiently high up in the troposphere where the temperature change in response to forcing is similar over land and ocean and the larger surface temperature response over land then is consistent with the different changes in lapse rates over land and ocean. Byrne and O'Gorman (2013a) formulate this effect in terms of the equality of equivalent potential temperature averaged over land and ocean as a result of weak temperature gradients in the free troposphere and convective quasi-equilibrium, which is largely supported by simulations with idealized climate models. However, they also notice that this equality breaks down in realistic climate models (Byrne & O'Gorman, 2013b) and the changes in the mean surface equivalent potential temperature, rather than the mean equivalent potential temperatures themselves, are more similar over land and ocean (Byrne & O'Gorman, 2013b, 2018). The importance of weak temperature gradients and convective quasi-equilibrium has also been emphasized by Chiang & Sobel, (2002, 2005) to explain the surface warming outside of the Pacific following the peak of an El Niño event.

In the following, we present observations and model results to provide a more precise picture of how tropical atmospheric dynamics couple the moist static energy (MSE; equivalent to the equivalent potential temperature used in Byrne & O'Gorman, 2013a, 2013b) of air near the surface over land and ocean to the free troposphere. We show that the subcloud MSE where convection occurs is roughly constant with latitude in the inner tropics (about 20° S to 20° N) and very similar over land and ocean, which may not be expected in light of the well-documented land-ocean contrast of tropical convection (Matsui et al., 2016; Robinson et al., 2011). Notably, this similarity holds across all latitudes of the inner tropics even on a daily timescale. As a result, the connection in subcloud MSE over land and ocean is only established in the highest MSE values that compose the convective regions.

2. Data and Method

2.1. Subcloud MSE

Subcloud MSE is computed using ERA-Interim 6-hourly reanalysis data on 0.75° × 0.75° grid and pressure levels (Dee et al., 2011). MSE h is calculated following the definition

$$h = c_p T + gz + Lq, \tag{1}$$

where c_p is the heat capacity of air, T is temperature, g is gravitational acceleration, z is height, L is the latent heat of vaporization of water, and q is the mixing ratio of water vapor. Standard values used in climate models and reanalysis data are adopted here, namely, c_p =1,005 J/kg/K, $L = 2.5\times10^6$ J/kg, and $g = 9.8$ m/s^2. The subcloud layer is the portion of the boundary layer extending from the surface to the average altitude of the base of clouds (American Meteorological Society, 2012). Here, we calculate the lifting condensation level as the pressure level closest to the first saturation point of an adiabatically lifted surface parcel on 6-hourly time frequency for every location and compare the LCLs to the 6-hourly boundary layer heights from ERA-Interim. Subcloud MSE is then the average MSE either within the layer between the ground and the LCL when the LCL is within the boundary layer, or within the boundary layer when the LCL is higher than the boundary layer top (no-cloud case). The 6-hourly subcloud MSE is averaged to a daily timescale to match the time resolution of the rainfall observation.

2.2. Convective Subcloud MSE

The convective (subcloud) MSE is calculated by weighting the daily-mean subcloud MSE in each grid box with the corresponding rainfall received, that is, rainfall intensity multiplied by the area of the grid box, following the rainfall-weighting method in Flannaghan et al. (2014) and Fueglistaler et al. (2015):

$$Convective \quad subcloud \quad MSE = \frac{\sum_i P_i h_i}{\sum_i P_i}. \tag{2}$$

To ensure robustness of our results, we estimate the convective MSE with different combinations of two reanalysis data sets (ERA-Interim and MERRA2; Rienecker et al., 2011) and two rainfall observation data sets (Tropical Rainfall Measuring Mission [TRMM] and GPCP; Huffman et al., 2001) on different timescales (daily and monthly), which yields very similar results (Text S1 and Figure S1 in the supporting information). In the following, we only show the combination of ERA-Interim and TRMM daily data. Daily rainfall observations from TRMM (Huffman et al., 2007) from 2001 to 2014 of 0.25° × 0.25° resolution are aggregated to the ERA-Interim grid conserving total precipitation fluxes. The convective (subcloud) MSE can be loosely interpreted as the subcloud MSE weighted by the mass flux transported from the subcloud layer to the free troposphere by deep convection, as convective mass flux scales roughly linearly with rainfall (Raymond et al., 2015). The resolution of the data used here (order 100 km) does not allow distinguishing between convective rain (1–10 km) and stratiform rain (~100 km) (Houze, 1997), which may introduce some ambiguity in the determination of convective MSE. For the convective MSE as a function of latitude, the subcloud MSE in each latitude band is first calculated on a yearly basis before averaging over the chosen period and hence is not influenced by trends or interannual variability in total tropical rainfall.

3. Results

3.1. The MSE Threshold for Convection—A Zeroth-Order Picture

The tropical atmosphere can be seen as consisting of a boundary layer with diverse temperature, humidity, and topography (the three components of MSE) and a free troposphere that is comparatively homogenous.

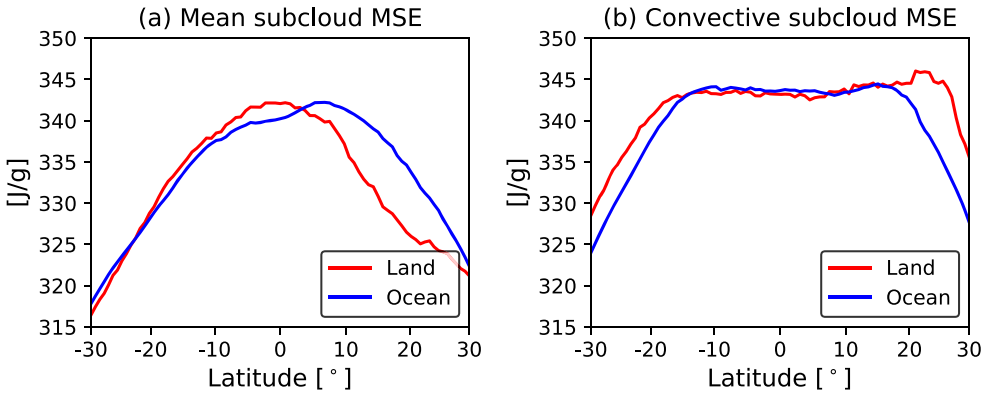

Figure 1. Zonal-mean (a) and convective (b) subcloud moist static energy (MSE) over land (red) and ocean (blue). Subcloud MSE is derived from ERA-Interim, and rainfall is from TRMM. Daily data from 2001 to 2014 are used. The convective subcloud MSE is determined by weighting the subcloud MSE at each longitude with the corresponding rainfall within each latitudinal band of 0.75° wide.

Deep convection transports boundary layer air upward into the free troposphere. Once the free troposphere is filled with buoyant air originating from the warm and humid boundary layer, it suppresses upward motion in the colder regions, establishing a threshold for convection. More quantitatively, the constraint from atmospheric dynamics can be expressed as a combination of convective quasi-equilibrium (QE) and weak temperature gradient (WTG) (Byrne & O'Gorman, 2013a), subsequently referred to as QE-WTG. Strict quasi-equilibrium assumes that convection maintains the subcloud MSE equal to the saturated MSE aloft in the free troposphere (e.g., Arakawa & Schubert, 1974; Emanuel, 2007) (The saturated MSE only strongly depends on the air temperature). Weak temperature gradient states that the free troposphere cannot sustain substantial horizontal temperature gradients due to the smallness of the Coriolis parameter in the tropics (e.g., Charney, 1963; Sobel & Bretherton, 2000). Consequently, at the limit of strict quasi-equilibrium and zero temperature gradient, simultaneously convecting regions, regardless of over land or ocean, should have the same subcloud MSE, which we refer to as the MSE threshold for convection. While previous studies (Byrne & O'Gorman, 2013a, 2013b, 2018) evaluate the QE-WTG picture with the large-scale mean MSE over land and ocean, we argue that QE-WTG should be evaluated only in the regions where deep convection couples the MSE in the subcloud layer to the free troposphere and does not apply to the regions where the sublcoud MSE is too low to reach the threshold for convection. Leveraging the aforementioned rainfall-weighting method, we are able show that QE-WTG apply to each latitude in the observations, even on a daily timescale, and there is a clear breakdown of the theoretical picture around 20° in both hemispheres.

The zonal-mean subcloud MSE (Figure 1a) peaks around the equator reflecting the annual mean solar forcing, whereas the convective subcloud MSE (Figure 1b) is roughly uniform throughout the inner tropics and very similar between land and ocean, reflecting the weak horizontal temperature gradients in the free troposphere. The sharp dropoff at about 20° in both hemispheres indicates where the Coriolis effect is no longer negligible and QE-WTG breaks down. Note that this emerging latitudinal range where QE-WTG work is consistent with the latitudinal range where the free tropospheric temperature variations are order 1 K (e.g., Fueglistaler et al., 2009). Conversely, the width of the equatorial wave guide is much narrower (e.g., Chiang & Lintner, 2005; Chiang & Sobel, 2002). As a result, rainfall in the subtropics can occur either at very low subcloud MSE when induced by the extratropical eddies (Funatsu & Waugh, 2008) or at very high subcloud MSE during the South Asian monsoon, which creates the peak in the convective MSE around 25° N over land (Boos & Kuang, 2010). Using subcloud MSE derived from MERRA2 instead of ERA-Interim does not change this result (Figure S2). The contrast between the mean and the convective subcloud MSE resolves the aforementioned inconsistency between the strict QE-WTG theory and the realistic simulations mentioned in Byrne and O'Gorman (2013b); convection only occurs in the part of the domain where the subcloud MSE is high enough to reach the tropically uniform MSE threshold of about 343 J/g shown in Figure 1b, and in the part of the domain that is not convecting, subcloud MSE is not coupled to the free troposphere and therefore can differ between land and ocean.

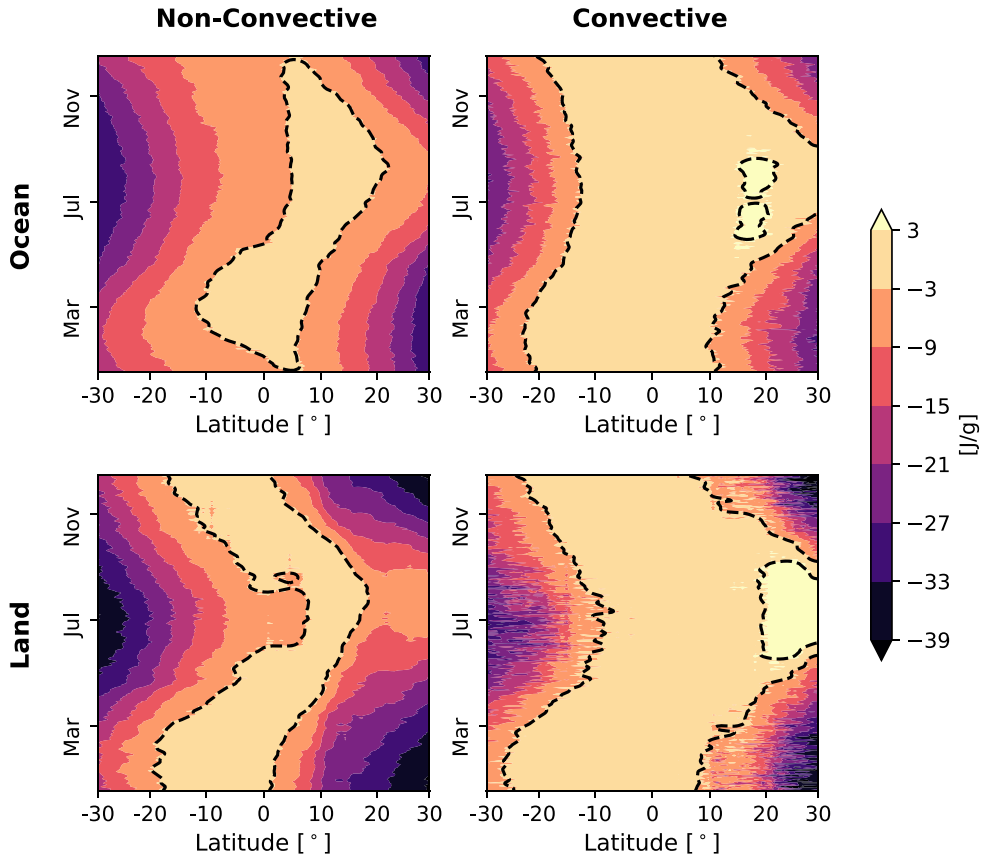

Figure 2. The mean subcloud moist static energy (MSE) as a function of latitude and day of year in the nonconvective and convective regions over ocean and land. A reference value for each day of year, calculated as the mean subcloud MSE in the convective regions over equatorial (5° S to 5° N) ocean, is subtracted from all panels. Daily data are used from ERA-Interim and TRMM between 2001 and 2014. Convective and nonconvective regions are identified with a rainfall threshold of 6 mm/day. The dashed contour lines indicate the subcloud MSE within ±3 J/g relative to the common reference value.

A more stringent test examines how effectively QE-WTG works on a daily basis. Figure 2 shows the seasonal evolution of the zonal-mean subcloud MSE in the convective regions (left column) and nonconvective regions (right column) over land (lower row) and ocean (upper row). Here the convective MSE is defined as the mean subcloud MSE where the rain rate is above 6 mm/day (Sobel et al., 2002) and vice versa for the nonconvective MSE. The results are not sensitive to the choice of a rainfall threshold from 2 to 20 mm/day (Figures S3 and S4). This method is different from the rainfall-weighting method used in Figure 1 but yields similar convective MSE values, essentially because rainfall anywhere in the inner tropics occurs at very similar subcloud MSE. To facilitate the comparison, a reference value for each day of year, calculated as the mean subcloud MSE in the convective regions over the equatorial (5° S to 5° N) ocean, is subtracted. Even on a single day of year, the convective MSE is still uniform over a broad range in latitude, though this latitudinal range has seasonality (Figure 2, right column). Within 20° S to 20° N, the seasonal evolution of the nonconvective MSE has more prominent land-ocean contrast than the convective MSE (indicated by the shapes of the dashed black contours), supporting the concept that only the subcloud MSE in the convective regions over land and ocean is tied to the uniform temperature in the free troposphere.

The physics involved in the QE-WTG mechanism does not rely on the mean climatic state; therefore, QE-WTG is expected to hold in all climates. Global climate models from the Coupled Model Intercomparison Project phase 5 (CMIP5) (Taylor et al., 2012) that correctly reproduce the observed uniform convective MSE in the simulations of the present climate (Figure S5 and Table S1) also show a uniform convective MSE in the projections of a much warmer climate under the Representative Concentration Pathway 8.5 (RCP8.5)

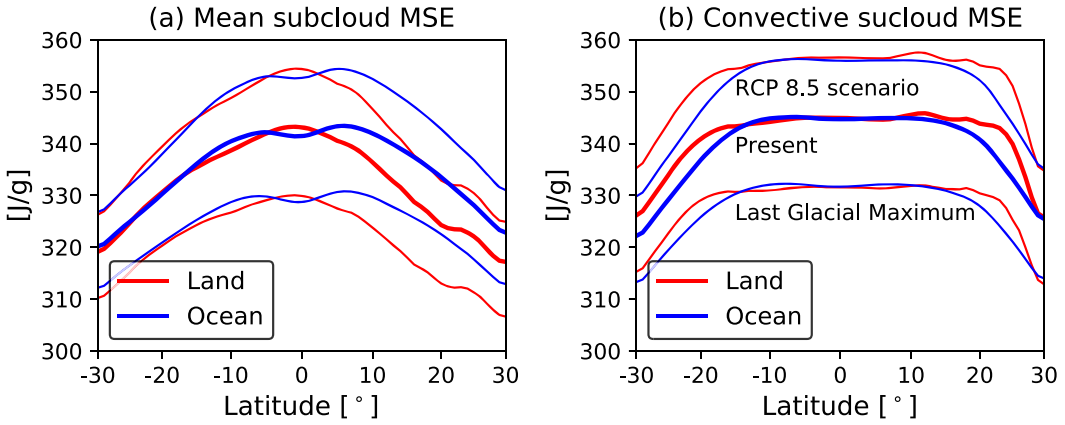

Figure 3. Zonal-mean (a) and convective (b) subcloud moist static energy (MSE) for model simulations. The multimodel mean of monthly data from CMIP5 models (see Table S1) are shown. Three experiments are shown from bottom to top: the Last Glacial Maximum, the period from 1979 to 2005 in the simulation of current climate (labeled "Present"), and the last 20 years of the 21st century in the global warming simulation (labeled "RCP 8.5 scenario").

emission scenario (Figure 3). Model simulations of the much colder Last Glacial Maximum also show a uniform convective MSE over both land and ocean. Therefore, Figure 3 demonstrates the validity of QE-WTG in a wide range of climates.

3.2. Finite Width of the MSE Threshold for Convection—A First-Order Correction

The latitudinal uniformity of the convective subcloud MSE in the inner tropics and its similarity between land and ocean (Figures 1 and 2) provide observational support for the zeroth-order picture. However, it is well established that factors such as the midtropospheric humidity (Brown & Zhang, 1997; Emanuel, 2019), convective inhibition (Mapes, 2000), low-level convergence (Back & Bretherton, 2009; Lindzen & Nigam, 1987), and stationary or transient equatorial waves (Gill, 1980; Kiladis et al., 2009) all affect the triggering of convection. How can these complicating factors by reconciled with the simple picture of a uniform MSE threshold for convection?

The convective MSE threshold shown in Figure 1b is a weighted mean over a range of subcloud MSE values rather than a single MSE value. Figure 4a shows the fraction of rainfall that falls into each subcloud MSE bin of a width of 0.2 J/g. This rainfall distribution can be roughly regarded as the convective mass flux distribution as a function of subcloud MSE. If QE-WTG were strict, this distribution would be a Dirac function at the highest subcloud MSE. In the observed climate, however, the majority of rainfall occurs around 343 J/g—the value is comparable to the convective MSE (Figure 1a)—with a half width at half maximum of 3 J/g. The half width of 3 J/g then encapsulates the previously mentioned factors that affect the local triggering of convection. This width is narrow compared to the entire range of the tropical subcloud MSE of about 60 J/g. Remarkably, the shape of the rainfall distribution as a function of subcloud MSE is also similar between land and ocean, a result not predicted by the theoretical limit of QE-WTG.

The tails of the rainfall distribution at very high subcloud MSE above 350 J/g and low subcloud MSE below 336 J/g are somewhat different for land and ocean, due to the breakdown of QE-WTG in the subtropics. When the latitudinal range is restricted to 20° S to 20° N (Figure 4c), the tails disappear, and a convective mode centered at 343 J/g emerges, which is almost identical over land and ocean.

Figure 4e is the same as Figure 4a but for the CMIP5 multimodel mean. The width of the MSE threshold is wider than that in the observations, because it is an average of models with slightly different mean states. In fact, the half width for an individual CMIP5 model is also 3 J/g on average. Limiting the latitudinal range to 20° S to 20° N for the CMIP5 models results in better agreement between land and ocean (not shown) similar to the observational result (Figures 4c and 4d).

To put the magnitude of the width into context, we compare it with typical MSE changes due to departure from the strict QE-WTG: Observed convective available potential energy varies between 0 and 4 J/g (Gettelman et al., 2002; Williams & Renno, 1993), and the free tropospheric temperature varies by order 1 K horizontally (e.g., Fueglistaler et al., 2009), which translates to about 2 J/g of subcloud MSE. It is thus not

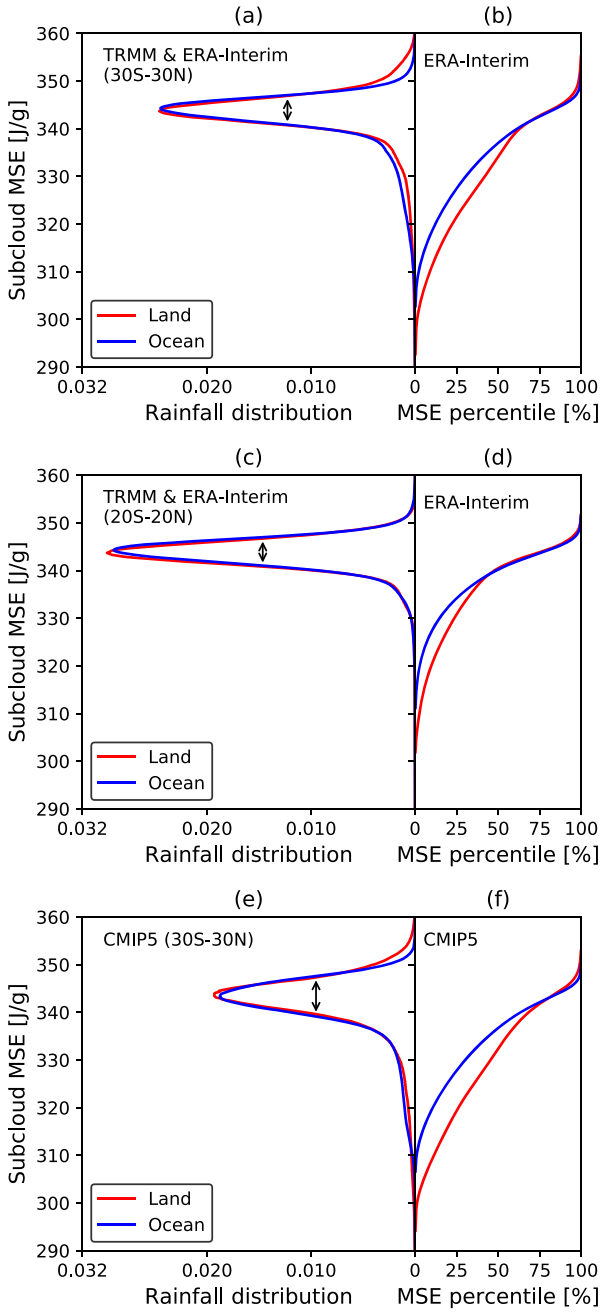

Figure 4. Rainfall distribution as a function of subcloud MSE (left panels) and the corresponding percentiles of subcloud MSE (right panels). (a and b) Rainfall from TRMM and subcloud MSE from ERA-Interim between 30° S and 30° N. (c and d) The same as (a) and (b) but with data between 20° S and 20° N. (e and f) The same as (a) and (b) but are the multimodel mean of monthly output from CMIP5 models in the coupled simulation from 1979 to 2005 (Table S1). The double arrows indicate where the HWHM is evaluated.

obvious which factor contributes more given the similar amplitudes. We also notice that the width is not strongly dependent on the time frequency (daily or monthly) of data.

Figures 4b, 4d, and 4f show the corresponding percentiles of subcloud MSE sorted in ascending order and averaged in equal-area bins. Figure 4b reiterates that only the highest subcloud MSE values between 30° S and 30° N are coupled over land and ocean while the low subcloud MSE values are free to differ—the upper 30% of subcloud MSE has almost identical distribution over land and ocean while the lower 70% of the subcloud MSE over ocean is systematically higher than that over land. In addition, Figures 4b and 4d

highlight an interesting aspect of the Earth's tropical climate: The convective area fraction is approximately equal over land and ocean.

4. Conclusion

We show that a simple theoretical picture of the tropical atmosphere based on the convective quasi-equilibrium and the weak temperature gradient assumptions (QE-WTG) can effectively explain the observations. In accordance with QE-WTG, the convective subcloud MSE is roughly constant with latitude between 20° S and 20° N on a daily timescale in the observed current climate and in the simulated past and future climates. The utility of QE-WTG is manifested in its capability of reconciling the land-ocean contrast. The vastly different land and ocean surfaces share almost identical convective subcloud MSE, distribution of highest subcloud MSE values, and precipitation distribution as a function of subcloud MSE. Whereas the role of subcloud MSE forcing the free troposphere has been well appreciated in tropical convection, we demonstrate that the horizontally uniform free tropospheric temperature forces the highest subcloud MSE values to be similar over land and ocean, which is an interesting aspect of convection in the tropics. These results fill the gap between the idealized, conceptual understanding of the tropical atmospheric dynamics and the real world consisting of diverse regional climates.

Acknowledgments
We thank Isaac Held and Nadir Jeevanjee for thoughtful feedback and discussion and Julius Busecke and Allison Hogikyan for suggestions on an earlier version of the manuscript. Y. Z. acknowledges support under award NA18OAR4320123 from the National Oceanic and Atmospheric Administration, U.S. Department of Commerce. The statements, findings, conclusions, and recommendations are those of the author(s) and do not necessarily reflect the views of the National Oceanic and Atmospheric Administration, or the U.S. Department of Commerce. S. F. acknowledges support from National Science Foundation Awards AGS-1417659 and AGS-1743753. We acknowledge the European Centre for Medium-range Weather Forecast (ECMWF) for providing ERA-Interim data (https://www.ecmwf.int/en/forecasts/datasets/archive-datasets/reanalysis-datasets/era-interim). We acknowledge the National Aeronautics and Space Administration (NASA) for providing Tropical Rainfall Measuring Mission (TRMM) 3B42 data (https://disc.gsfc.nasa.gov/datasets/TRMM_3B42RT_Daily_V7/summary). We acknowledge the World Climate Research Programme's Working Group on Coupled Modelling and climate modeling groups (Table S1) for producing CMIP5 model data (https://esgf-node.llnl.gov/projects/cmip5).

References

American Meteorological Society (2012). Subcloud layer, glossary of meterology. (http://glossary.ametsoc.org/wiki/Subcloudlayer, Last accessed on 2019-11-2).

Arakawa, A., & Schubert, W. H. (1974). Interaction of a cumulus cloud ensemble with the large-scale environment, Part I. *Journal of the Atmospheric Sciences*, *31*(3), 674–701.

Back, L., & Bretherton, C. (2009). On the relationship between SST gradients, boundary layer winds, and convergence over the tropical oceans. *Journal of Climate*, *22*, 4182–4196. https://doi.org/10.1175/2009JCLI2392.1

Boos, W., & Kuang, Z. (2010). Dominant control of the South Asian monsoon by orographic insulation versus plateau heating. *Nature*, *463*, 218–222.

Brown, R. G., & Zhang, C. (1997). Variability of midtropospheric moisture and its effect on cloud-top height distribution during TOGA COARE. *Journal of the Atmospheric Sciences*, *54*(23), 2760–2774.

Byrne, M. P., & O'Gorman, P. A. (2013a). Land-ocean warming contrast over a wide range of climates: Convective quasi-equilibrium theory and idealized simulations. *Journal of Climate*, *26*(12), 4000–4016.

Byrne, M. P., & O'Gorman, P. A. (2013b). Link between land-ocean warming contrast and surface relative humidities in simulations with coupled climate models. *Geophysical Research Letters*, *40*, 5223–5227. https://doi.org/10.1002/grl.50971

Byrne, M. P., & O'Gorman, P. A. (2015). The response of precipitation minus evapotranspiration to climate warming: Why the "wet-get-wetter, dry-get-drier" scaling does not hold over land. *Journal of Climate*, *28*(20), 8078–8092.

Byrne, M. P., & O'Gorman, P. A. (2018). Trends in continental temperature and humidity directly linked to ocean warming. *Proceedings of the National Academy of Sciences*, *115*(19), 4863–4868.

Charney, J. (1963). A note on large-scale motions in the tropics. *Journal of the Atmospheric Sciences*, *20*, 607–609.

Chiang, J. C., & Lintner, B. R. (2005). Mechanisms of remote tropical surface warming during El Niño. *Journal of climate*, *18*(20), 4130–4149.

Chiang, J. C., & Sobel, A. H. (2002). Tropical tropospheric temperature variations caused by ENSO and their influence on the remote tropical climate. *Journal of climate*, *15*(18), 2616–2631.

Dee, D. P., Uppala, S., Simmons, A., Berrisford, P., Poli, P., Kobayashi, S., et al. (2011). The ERA-Interim reanalysis: Configuration and performance of the data assimilation system. *Quarterly Journal of the royal meteorological society*, *137*(656), 553–597.

Emanuel, K. (2007). Quasi-equilibrium dynamics of the tropical atmosphere. *The Global Circulation of the Atmosphere*, 186–218.

Emanuel, K. (2019). Inferences from simple models of slow, convectively coupled processes. *Journal of the Atmospheric Sciences*, *76*(1), 195–208.

Flannaghan, T. J., Fueglistaler, S., Held, I. M., Po-Chedley, S., Wyman, B., & Zhao, M. (2014). Tropical temperature trends in atmospheric general circulation model simulations and the impact of uncertainties in observed SSTs. *Journal of Geophysical Research: Atmospheres*, *119*, 13,327–13,337. https://doi.org/10.1002/2014JD022365

Fueglistaler, S., Dessler, A. E., Dunkerton, T. J., Folkins, I., Fu, Q., & Mote, P. W. (2009). Tropical tropopause layer. *Reviews of Geophysics*, *47*, RG1004. https://doi.org/10.1029/2008RG000267

Fueglistaler, S., Radley, C., & Held, I. M. (2015). The distribution of precipitation and the spread in tropical upper tropospheric temperature trends. *Geophysical Research Letters*, *42*, 6000–6007. https://doi.org/10.1002/2015GL064966

Funatsu, B., & Waugh, D. (2008). Connections between potential vorticity intrusions and convection in the Eastern Tropical Pacific. *Journal of the Atmospheric Sciences*, *65*, 987–1002. https://doi.org/10.1175/2007JAS2248.1

Gettelman, A., Seidel, D., Wheeler, M., & Ross, R. (2002). Multidecadal trends in tropical convective available potential energy. *Journal of Geophysical Research*, *107*, D21.

Gill, A. E. (1980). Some simple solutions for heat-induced tropical circulation. *Quarterly Journal of the Royal Meteorological Society*, *106*(449), 447–462.

Houze, R. (1997). Stratiform Precipitation in regions of convection: A meteorological paradox? *Bulletin American Meteorological Society*, *78*(10), 2179–2196.

Huffman, G. J., Adler, R. F., Morrissey, M. M., Bolvin, D. T., Curtis, S., Joyce, R, & Susskind, J. (2001). Global precipitation at one-degree daily resolution from multisatellite observations. *Journal of Hydrometeorology*, *2*(1), 36–50. https://doi.org/10.1175/1525-7541(2001)0022.0.co;2

Huffman, G. J., Bolvin, D. T., Nelkin, E. J., Wolff, D. B., Adler, R. F., Gu, G., & Stocker, E. F. (2007). The TRMM multisatellite precipitation analysis (TMPA): Quasi-global, multiyear, combined-sensor precipitation estimates at fine scales. *Journal of hydrometeorology*, *8*(1), 38–55.

Joshi, M. M., Gregory, J. M., Webb, M. J., Sexton, D. M. H., & Johns, T. C. (2008). Mechanisms for the land/sea warming contrast exhibited by simulations of climate change. *Climate Dynamics*, *30*, 455–465.

Kiladis, G. N., Wheeler, M., Haertel, P., Straub, K., & Roundy, P. (2009). Convectively coupled equatorial waves. *Reviews of Geophysics*, *47*, RG2003. https://doi.org/10.1029/2008RG000266

Lindzen, R., & Nigam, S. (1987). On the role of sea surface temperature gradients in forcing low-level winds and convergence in the tropics. *Journal of the Atmospheric Sciences*, *44*(17), 2418–2436.

Lintner, B. R., & Chiang, J. C. (2005). Reorganization of tropical climate during El Nino: A weak temperature gradient approach. *Journal of climate*, *18*(24), 5312–5329.

Manabe, S., Stouffer, R., Spelman, M., & Bryan, K. (1991). Transient responses of a coupled ocean-atmosphere model to gradual changes of atmospheric CO2. Part I: Annual mean response. *Journal of Climate*, *4*, 785–818.

Mapes, B. E. (2000). Convective inhibition, subgrid-scale triggering energy, and stratiform instability in a toy tropical wave model. *Journal of the Atmospheric Sciences*, *57*(10), 1515–1535.

Matsui, T., Chern, J. D., Tao, W. K., Lang, S., Satoh, M., Hashino, T., & Kubota, T. (2016). On the land-ocean contrast of tropical convection and microphysics statistics derived from TRMM satellite signals and global storm-resolving models. *Journal of Hydrometeorology*, *17*(5), 1425–1445.

Pendergrass, A. G., Knutti, R., Lehner, F., Deser, C., & Sanderson, B. M. (2017). Precipitation variability increases in a warmer climate. *Scientific reports*, *7*(1), 17966.

Raymond, D., Fuchs, Z., Gjorgjievska, S., & Sessions, S. (2015). Balanced dynamics and convection in the tropical troposphere. *Journal of Advances in Modeling Earth Systems*, *7*, 1093–1116. https://doi.org/10.1002/2015MS000467

Rienecker, M. M., Suarez, M. J., Gelaro, R., Todling, R., Bacmeister, J., Liu, E, & Woollen, J. (2011). MERRA: NASA's Modern-Era Retrospective Analysis for Research and Applications. *Journal of Climate*, *24*(14), 3624–3648. https://doi.org/10.1175/jcli-d-11-00015.1

Robinson, F., Sherwood, S., Gerstle, D., Liu, C., & Kirshbaum, D. J. (2011). Exploring the land-ocean contrast in convective vigor using islands. *Journal of the Atmospheric Sciences*, *68*(3), 602–618.

Seneviratne, S. I., Wilhelm, M., Stanelle, T., van den Hurk, B., Hagemann, S., Berg, A., et al. (2013). Impact of soil moisture-climate feedbacks on CMIP5 projections: First results from the GLACE-CMIP5 experiment. *Geophysical Research Letters*, *40*, 5212–5217. https://doi.org/10.1002/grl.50956

Sobel, A. H., & Bretherton, C. S. (2000). Modeling tropical precipitation in a single column. *Journal of Climate*, *13*(24), 4378–4392.

Sobel, A., Held, I., & Bretherton, C. (2002). The ENSO signal in tropical tropospheric temperature. *Journal of Climate*, *15*(18), 2702–2706.

Taylor, K. E., Stouffer, R. J., & Meehl, G. A. (2012). An overview of CMIP5 and the experiment design. *Bulletin of the American Meteorological Society*, *93*(4), 485–498.

Williams, E., & Renno, N. (1993). An analysis of the conditional instability of the tropical atmosphere. *Monthly Weather Review*, *121*(1), 21–36.